Vaccine xxx (2015) xxx–xxx

Contents lists available at ScienceDirect

Vaccine

journal homepage: www.elsevier.com/locate/vaccine

Broad spectrum assessment of the epitope fluctuation—Immunogenicity hypothesis

Jason S. Grosch, Jing Yang [1], Alice Shen [1], Yuriy V. Sereda [1], Peter J. Ortoleva *

Center for Theoretical and Computational Nanoscience, Department of Chemistry Indiana University, Bloomington, IN 47405, United States

ARTICLE INFO

Article history:
Available online xxx

Keywords:
Vaccine
Nanoparticles
Epitope
Immunogenicity
Computer-aided design
Bioinformatics

ABSTRACT

Prediction of immunogenicity is a substantial barrier in vaccine design. Here, a molecular dynamics approach to assessing the immunogenicity of nanoparticles based on structure is presented. Molecular properties of epitopes on nonenveloped viral particles are quantified via a set of metrics. One such metric, epitope fluctuation (and implied flexibility), is shown to be inversely correlated with immunogenicity for each of a broad spectrum of nonenveloped viruses. The molecular metrics and experimentally determined immunogenicities for these viruses are archived in the open-source vaccine computer-aided design database. Results indicate the promise of computer-aided vaccine design to bring greater efficiency to traditional lab-based vaccine discovery approaches.

1. Introduction

Nanoparticle-based vaccines are in widespread use or in various stages of development [1–3]. For example, human papillomavirus (HPV) [4,5] and hepatitis E virus (HEV) [6] vaccines are based on virus-like particles (VLPs) and are in clinical use. VLPs are noninfectious nanoparticles that display the key structural features of native target viruses and induce a high immune response [7]. Here, a correlation between properties of VLPs predicted by molecular dynamics computations and experimentally determined immunogenicity is presented.

A priori, it is challenging to predict whether a vaccine candidate can induce a neutralizing antibody response. Recently, there have been advances in systems biology to predict vaccine efficacy, but there does not seem to be methods that relate molecular properties to vaccine immunogenicity [8]. In experimental studies, a positive correlation between immunogenicity and increasing nanoparticle assembly size has been observed [9]. For instance, HPV VLPs exhibit higher immunogenicity than subunit assemblies, proteins, or peptides extracted from the same target virus (Fig. 1) [9]. These findings seem to suggest that larger viral protein assemblies elicit stronger immune responses, even after accounting for differences in total number of epitopes delivered (i.e. the dosage effect). However, Varsani et al. [10] showed that the immune response can vary with epitope position on the same VLP. In summary, these studies imply that there may be a correlation between VLP molecular-scale properties and immunogenicity that changes with VLP assembly size.

In computational studies of HPV VLPs, the intensity of fluctuations expressed by epitopes decreased across monomers, pentamers, and VLPs, respectively [11]. Moreover, the degree of epitope fluctuation was observed to have an inverse relationship with antibody binding energy in flaviviruses [12]. These results suggest that computationally predicted epitope fluctuation can serve as a molecular indicator of vaccine immunogenicity. Other molecular metrics that could be predictive of immunogenicity include epitope density (i.e. the number of epitopes presented per particle) [13]. It has been proposed that VLPs have a greater ability than lower-order assemblies (monomers, pentamers, etc.) to present epitopes in a packed array, which encourages B-cell receptor cross linking and a stronger immune response [14].

Computer-aided vaccine design holds promise for reducing the immense amount of time and cost of experimental vaccine discovery. Currently, most bioinformatics approaches to vaccine design focus on antigen prediction via sequence alignment algorithms [15–17]. Such methods can be effective for T-cell epitope discovery [15,16], and there has been some effort to link the number of predicted epitopes per particle to immunogenicity [8]. However, these methods are not effective at discovering B-cell epitopes [18–20], which is required for a strong neutralizing antibody response [21]. These methods provide information on epitope location, but not on vaccine efficacy.

The present study introduces a vaccine computer-aided design (VCAD) method to quantify the relationship between molecular properties and immunogenicity. Here, the epitope

* Corresponding author. Tel.: +1 8128566000.
E-mail address: ortoleva@indiana.edu (P.J. Ortoleva).
[1] These authors contributed equally.

http://dx.doi.org/10.1016/j.vaccine.2015.06.111
0264-410X/

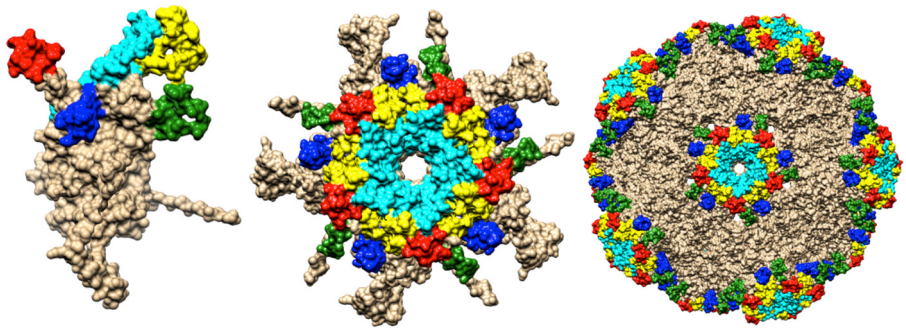

Fig. 1. The HPV VLP assembly hierarchy: (a) monomer, (b) pentamer, and (c) VLP. Epitopes are highlighted: BC (blue), DE (cyan), EF (green), FG (yellow), and HI (red).

fluctuation–immunogenicity hypothesis [11,22]—a proposed inverse correlation between immunogenicity and epitope fluctuation intensity—is assessed using a spectrum of nonenveloped viruses. This study represents the first attempt to link computationally predicted molecular properties and experimentally derived immunogenicity for a spectrum of viruses. Molecular dynamics (MD) was used to simulate VLPs of these nonenveloped viruses and correlations are made between intrinsic properties of their epitopes and experimentally derived immunogenicity.

2. Methods and materials

2.1. Nanoparticle assemblies and molecular dynamics simulations

Atomic coordinates for HPV 16 L1 coat protein [23], HEV VLP [24], human enterovirus (EV) A71 [25], poliovirus (PV) types 1 [26] and 3 [27] nanoparticle assemblies were obtained from crystal structures available in the RCSB Protein Data Bank [28]. A monomer and VLP were constructed for HEV. For EV A71, the following were constructed: peptides (residues 211–225 and 136–150), monomers (VP1 and VP2), pentamer, and VLP. For PV1, the following were constructed: peptides (residues 121–141, 182–201, and 270–287), monomers (VP2 and VP3), pentamer, and VLP. Only the VLP was constructed for PV3. A monomer, pentamer, and VLP were constructed for HPV 16. VLPs were constructed using monomer information from the RCSB Protein Data Bank and ViperDB [29].

HEV, EV, and PVs were solvated using TIP3P water and 0.3 M NaCl through the VMD 1.9.2 Autoionize 1.3 plugin [30,31]. Each one was placed in the center of the solution, and was separated by at least 1.0 nm from the box wall. Periodic boundary conditions were used, with at least 2.0 nm of water between images. System sizes varied in the range of $\sim 10^5$–10^6 atoms. The short-range cutoff was set to 1.2 nm with a switching function starting at 1.0 nm. The long-range electrostatics was handled using the particle mesh Ewald's method with a grid spacing of 1.0 Å. A constant temperature of 300 K was maintained using Langevin dynamics with a damping coefficient of 5 ps for nonhydrogen atoms. A constant pressure of 1 atm was maintained using the Nose-Hoover Langevin piston with a period of 100 fs and a damping time scale of 50 fs. 1 fs time steps were used and data was collected every 1 ps.[32] Using NAMD 2.9 [33] with the CHARMM27 force field [34], steepest decent energy minimization and equilibration were applied for each system prior to simulation. Each system was equilibrated until the RMSD relative to the initial structure was approximately constant and the potential energy was minimized. The RMSD was calculated as follows:

$$\sqrt{\frac{1}{N}\sum_{n=1}^{N}|r_n - r_{n,\mathrm{ref}}|^2} \tag{1}$$

Where r_n is the position of backbone atom n and $r_{n,\mathrm{ref}}$ is the position of the reference for atom n. Production runs were 5 ns in duration after the RMSD was constant.

To determine whether calculated molecular quantities (Section 2.2) were sensitive to computational conditions, HPV 16 was simulated under different conditions than the previous viruses. Each HPV 16 structure was solvated using SPC/E water [35] and 0.142 M NaCl using GROMACS 4.6.5 [36]. Each viral structure used the GROMOS 54A7 force field and was at least 1.4 nm from the box wall [37]. Steepest decent energy minimization and equilibration were performed for each system prior to each of the production runs, as above. A constant temperature of 300 K was maintained using the v-rescale thermostat [38] with a 0.1 ps coupling time and the Parrinello–Rahman barostat [39] with a 1 ps relaxation time. Hydrogen bonds were fixed using the LINCS algorithm [40], allowing for 2 fs time steps. Production runs were 5 ns in duration.

2.2. Selection of intrinsic metrics

Mean square fluctuations (MSF) and solvent accessible surface area (SASA) were calculated to correlate them with experimental immunogenicity. These metrics were chosen because MSF can measure epitope flexibility, which has been shown experimentally to mediate binding between epitopes and antibodies [41–43]. SASA was chosen because epitopes must be accessible to bind with antibodies. Therefore, it might be hypothesized that the most solvent accessible epitopes elicit the strongest immune responses.

2.2.1. Mean square fluctuations

An inverse correlation between MSF and immunogenicity was hypothesized for HPV VLPs and possibly for other systems [11,44]. Large MSF values indicate high epitope flexibility, resulting in conformational epitopes in improper orientations and unable to bind effectively to immune cell surface receptors [45–47]. MSF was calculated with center of mass translation and rotation removed via the following formula:

$$\frac{1}{N}\sum_{n=1}^{N}\frac{1}{T}\sum_{t=1}^{T}|\vec{r}_n(t) - \langle\vec{r}_n\rangle|^2 \tag{2}$$

where $\vec{r}_n(t)$ is the position of backbone atom n of a residue with N backbone atoms at time t and $\langle\vec{r}_n\rangle$ is the time average position of atom n and T is the number of discrete time steps. For a pentamer or larger assembly, each of its monomers were analyzed separately and averaged.

2.2.2. Solvent accessible surface area

High SASA of epitopes is hypothesized to be a necessary, though not sufficient, condition for epitopes to elicit a neutralizing antibody response. From this perspective, SASA would be expected to be positively correlated with immunogenicity. SASA is computed via the "rolling ball" algorithms implemented in GROMACS by g_sas,

Please cite this article in press as: Grosch JS, et al. Broad spectrum assessment of the epitope fluctuation—Immunogenicity hypothesis. Vaccine (2015), http://dx.doi.org/10.1016/j.vaccine.2015.06.111

Table 1
Binned immunogenicity for each simulated system [9,49–59].

System	Immunogenicity
EV mon VP1	0.25
EV mon VP2	0.25
EV peptide VP1	0
EV peptide VP2	0
EV VLP	1
HEV mon	0.25
HEV VLP	1
HPV mon	0.25
HPV pent	0.5
HPV VLP	1, 1
PV1 peptide 121–141	0
PV1 peptide 182–201	0.25
PV1 peptide 270–287	0
PV1 pent	0.75
PV1 VLP	1
PV1 VP2 mon	0.5
PV1 VP3 mon	0.5
PV3 VLP	0.75

wherein the nanoparticle surface is probed with a sphere of 0.7 nm radius [48].

2.2.3. Immunogenicity

The immunogenicity of each system was estimated based on published experimental titer values. Viruses included are HPV 16 [9], HEV [49–51], EV A71 [52,53], and PVs 1 [54–58] and 3 [59]. Based on the immunogenic responses, the data were binned into values of 0, 0.25, 0.5, 0.75, or 1 for nonimmunogenic, weakly immunogenic, moderately immunogenic, strongly immunogenic, and successful vaccine. Because of widely varying experimental conditions (different solvents, adjuvants, etc.) and the semiquantitative nature of some experiments, it is difficult to quantitatively correlate measured titer values to immunogenicity. Thus, the above binning of the disparate experimental data was required to make a correlation between immunogenicity and molecular metrics. The binned immunogenicity for each system is listed in Table 1.

A nonimmunogenic region (sequence) of each protein was used as a control for each metric. The selection of residues for each system is listed in Table 3. These regions were chosen to be inaccessible to external molecules, thus preventing them from being immunogenic. If a given metric shows a correlation with immunogenicity then this control experiment is expected to yield no correlation.

2.3. The VCAD database

The calculated data was archived in the VCAD database (http://io.chem.indiana.edu/vaccineCAD/). The VCAD database archives the following information for each virus studied: nanoparticle structural data, antibody data, computed molecular metrics, immunogenicity, and input files for MD simulations.

3. Results

Analysis of the backbone RMSD (Fig. 2) shows that the systems were equilibrated prior to the calculation of molecular metrics. The profiles of MSF as a function of residue number for HPV 16 pentamer show that simulations longer than 5 ns did not indicate significant change in the time average epitope MSF (Fig. 3). Thus, 5 ns was chosen as a sufficient time for collecting average values. The MSF of known epitopes (Table 2) for each system was obtained by averaging the MSF of each residue within the epitope. (Table 3).

The average MSF of each epitope was plotted against experimental immunogenicity found in the literature (Fig. 4) [9,49,51–59]. This was compared with the plot of SASA against immunogenicity

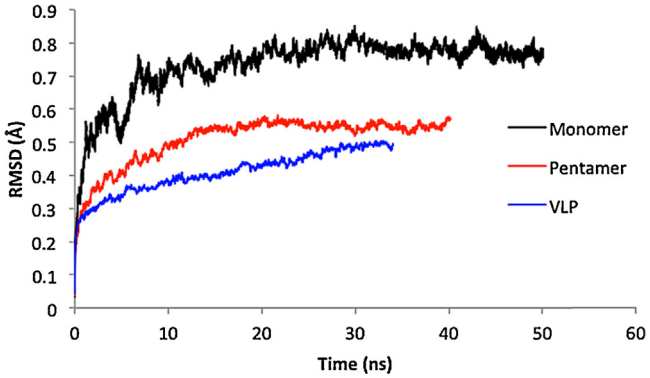

Fig. 2. Each system (HPV 16 shown here), was simulated until the backbone RMSD was constant. Molecular metrics were calculated using the last 5 ns.

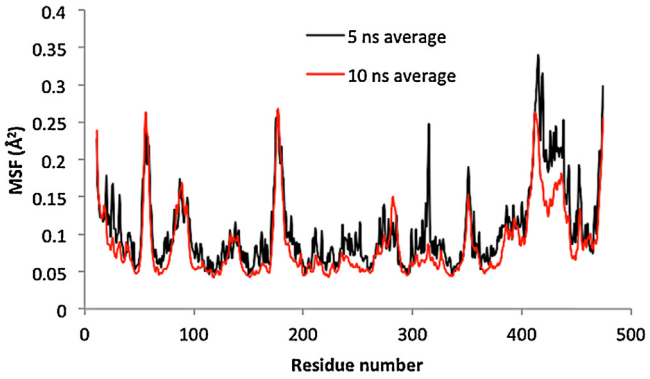

Fig. 3. MSF profiles of HPV 16 pentamer show that increased time averaging beyond 5 ns does not change the profiles significantly at the epitope from residues 170–189. Thus, 5 ns was deemed sufficient for calculating molecular metrics for other systems.

Table 2
List of epitopes used for the molecular metrics calculations [9,49–59].

System	Epitope residues
PV1 (VP2)	164–170, 270
PV1 (VP3)	58–60, 70–73, 76, 77, 79
PV1 (VP3)	58–60, 70–73, 76, 77, 79
PV3	89–100
HEV	452–617
HPV 16	170–189
EV 71 (VP1)	163–177
EV 71 (VP2)	136–150

Table 3
List of nonimmunogenic sequences used for the molecular metrics calculations.

System	Epitope residues
PV1 (VP2)	103–123
PV1 (VP3)	80–100
PV3	260–270
HEV	368–398
HPV	220–230
EV 71 (VP1)	148–168
EV 71 (VP2)	60–80

(Fig. 5). Nonimmunogenic regions of the proteins were used as a control for each metric (Figs. 6 and 7).

4. Discussion

The relationship between immunogenicity and MSF shows an inverse correlation (Fig. 4). The binned immunogenicity from titer to unitless values ranging from 0 to 1 introduces a course-grained

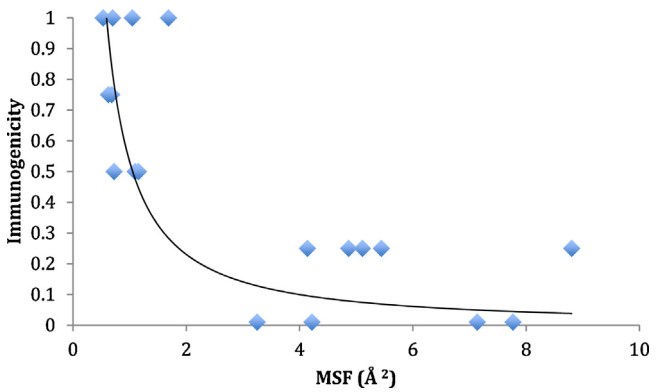

Fig. 4. Experimentally determined immunogenicity is inversely correlated with calculated MSF, a measure of flexibility. Error values are in Table S1.

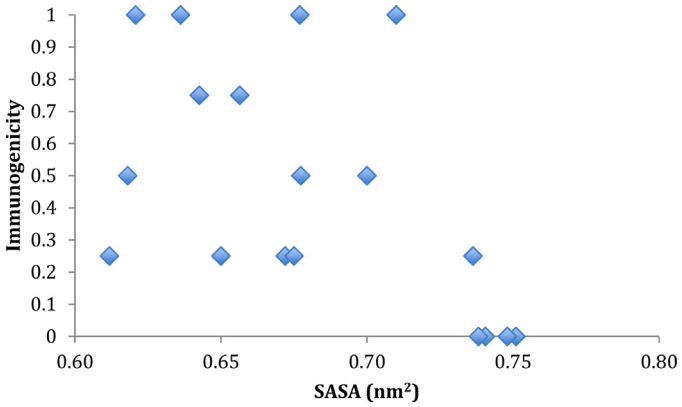

Fig. 5. Viral immunogenicity shows no correlation with calculated SASA. Error values are in Table S2.

perspective, but a strong trend is still evident. This perspective is consistent with the semiquantitative nature of experimentally evaluated and heterogeneity immunogenicity. Compared with the inverse correlation between immunogenicity and MSF, SASA has little correlation with immunogenicity (Fig. 5). Comparison of Figs. 4 and 5 provide a method to evaluate whether the binned immunogenicity introduced a systematic bias to the data. If the binned immunogenicity created an artificial trend then it is expected to appear in both the MSF and SASA plots, which is not the case. Thus, despite the uncertainty introduced by binning titer values, the strong correlation suggests that calculated MSF is a

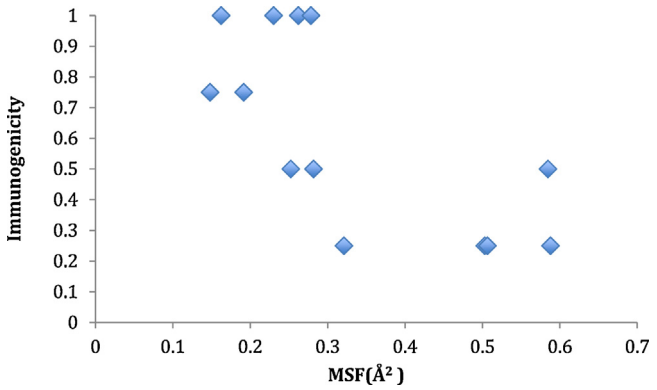

Fig. 6. Immunogenicity is not correlated with the MSF of nonimmunogenic sequences. Each sequence is not surface exposed and is presumably of very low imunogenicity. This provides a control for the MSF measurements shown in Fig. 4. Peptides were not included in this dataset. Error values are in Table S3.

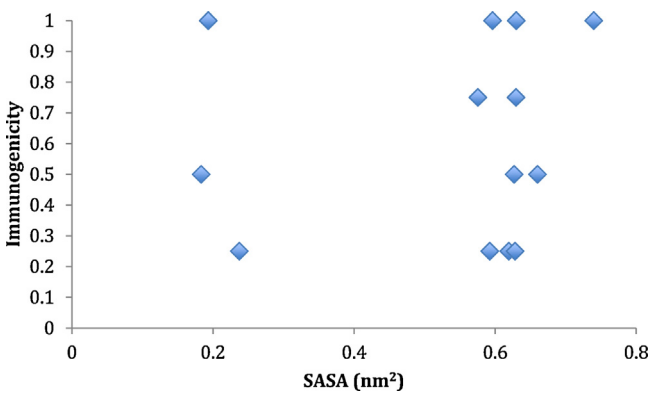

Fig. 7. Immunogenicity is not correlated with the SASA of nonimmunogenic sequences. Each sequence is not surface exposed and is presumably of very low imunogenicity. This provides a control for the SASA measurements shown in Fig. 5. Error values are in Table S4.

reliable predictor of immunogenicity. The uncertainty introduced by binning the immunogenicity prevents Fig. 4 from being used quantitatively to predict experimental titer values. However, the MSF–immunogenicity relationship can be used semiquantitatively to discriminate between high- and low-immunogenic vaccine candidates.

The relationship between calculated MSF and experimentally determined immunogenicity is confirmed by using nonimmunogenic sequences as a negative control. Fig. 6 shows that high- and low-immunogenic structures cannot be readily distinguished for nonepitope regions of the proteins. These residues are an excellent control because they are in positions that cannot readily interact with antibodies and are thus likely nonimmunogenic, whereas residues fully exposed on the surface may be an unidentified epitope. Fig. 7 confirms the absence of a relationship between immunogenicity and SASA. These controls provide verification that MSF, and its implied flexibility, is an indicator of immunogenicity and that solvent accessibility is not.

The absence of a relationship between SASA and immunogenicity (within the range studied) is unexpected because a key aspect of epitopes and other antigens is being solvent accessible to have effective interactions with antibodies. This shows that being solvent accessible, while necessary to be an epitope, is not sufficient for it to be strongly interacting. The inverse correlation between epitope MSF and immunogenicity suggests that epitope flexibility is a major predictor of immunogenicity. As MSF is a measure of deviation from an average structure over time, highly flexible epitopes will have higher MSF because of greater deviations from their time averaged structures. As the effectiveness of the interaction between a B-cell epitope and an antibody are highly sensitive to the three-dimensional shape of the epitope [60,61], more flexible B-cell epitopes have a greater probability to be in suboptimal conformation for interaction. Recently, this concept was explored experimentally, where it was shown that rigid B-cell epitopes in HIV-1 gp140 protein resulted in increased antibody binding [62]. This suggests that correlations such as in Fig. 4 could also be developed for enveloped viruses.

The MSF profiles are only reproducible when MD simulations are carried to equilibrium. Prior to equilibration of the epitopes, their MSF profiles can change significantly because overall epitope deformation accompanying approach to equilibrium can mask the fluctuation. The trend of decreasing MSF with increasing immunogenicity was found using both the CHARMM and GROMOS force fields. This suggests that the characterization of epitope flexibility by MD to discriminate between high- and low-immunogenic vaccine candidates is not an artifact of the force field used. If the

Please cite this article in press as: Grosch JS, et al. Broad spectrum assessment of the epitope fluctuation–Immunogenicity hypothesis. Vaccine (2015), http://dx.doi.org/10.1016/j.vaccine.2015.06.111

correlation of Fig. 4 is applicable to a broad spectrum of nonenveloped viruses, force-field independence is expected.

The calculated data for immunogenicity as a function of MSF have been made publicly available at the VCAD database at http://io.chem.indiana.edu/vaccineCAD/. Data archived include information on nanoparticle and antibody structure, computed molecular metrics, laboratory determined immunogenicity, and input files and output files for MD simulations. Because the VCAD database is regularly updated, it is expected that the correlation will improve over time. Similarly, the addition of multiple reliable molecular metrics should improve the accuracy of immunogenicity prediction.

5. Conclusions

An extensive study of the immunogenicity–fluctuation hypothesis showed that there is an inverse correlation between experimental immunogenicity and computationally calculated MSF for a spectrum of simulated nonenveloped viruses. The relationship can be used semiquantitatively to discriminate between high- and low-immunogenic vaccine candidates. This study advances computational vaccinology, which traditionally focuses on epitope discovery. The data here, including input and output files, have been made publicly available through the VCAD database (http://io.chem.indiana.edu/vaccineCAD/). It is suggested that the discovery of other types of vaccines (e.g. for enveloped viruses and cancer) are expected to follow from this study.

Acknowledgments

This research was supported in part by the following: NSF INSPIRE program under Grant No. ECCS-1344263; Indiana University College of Arts and Science via the Center for Theoretical and Computational Nanoscience; Lilly Endowment, Inc., through its support for the Indiana University Pervasive Technology Institute and the Indiana METACyt initiative.

Appendix A. Supplementary data

Supplementary data associated with this article can be found, in the online version, at doi:10.1016/j.vaccine.2015.06.111

References

[1] Park Y-M, Lee SJ, Kim YS, Lee MH, Cha GS, Jung ID, et al. Immune Netw 2013;13(5):177–83.
[2] Zhao Q, Li S, Yu H, Xia N, Modis Y. Trends Biotechnol 2013;31(11):654–63.
[3] Roldão A, Mellado MCM, Castilho LR, Carrondo MJT, Alves PM. Expert Rev Vaccines 2010;9(10):1149–76.
[4] Shi L, Sings HL, Bryan JT, Wang B, Wang Y, Mach H, et al. Clin Pharmacol Ther 2007;81(2):259–64.
[5] Monie A, Hung C. Biologics 2008;2(1):107–13.
[6] Park SB. Nature 2012;491(7422):21–2.
[7] Zeltins A. Mol Biotechnol 2013;53(1):92–107.
[8] Groot AS De, Moise L. Curr Opin Drug Discov Dev 2007.
[9] Thönes N, Herreiner A, Schädlich L, Piuko K, Müller M. J Virol 2008;82(11):5472–85.
[10] Varsani A, Williamson A-L, de Villiers D, Becker I, Christensen ND, Rybicki EP. J Virol 2003;77(15):8386–93.
[11] Joshi H, Cheluvaraja S, Somogyi E, Brown DR, Ortoleva P. Vaccine 2011;29(51):9423–30.
[12] Maillard RA, Liu T, Beasley DWC, Barrett ADT, Hilser VJ, Lee JC. J Am Chem Soc 2014;136(29):10315–24.
[13] Liu W, Chen Y-H. Eur J Immunol 2005;35(2):505–14.
[14] Alla S, Raychaudhuri S. J Immunol 2010;184(1), 130.2.
[15] Tong JC, Tan TW, Ranganathan S. Brief Bioinform 2007;8(2):96–108.
[16] Li Pira G, Ivaldi F, Moretti P, Manca F. J Biomed Biotechnol 2010;2010:325720.
[17] Koren E, De Groot AS, Jawa V, Beck KD, Boone T, Rivera D, et al. Clin Immunol 2007;124(1):26–32.
[18] Weber CA, Mehta PJ, Ardito M, Moise L, Martin B, De Groot AS. Adv Drug Deliv Rev 2009;61(11):965–76.
[19] Kringelum JV, Lundegaard C, Lund O, Nielsen M. PLoS Comput Biol 2012;8(12):e1002829.
[20] Haste Andersen P, Nielsen M, Lund O. Protein Sci 2006;15(11):2558–67.
[21] Bachmann MF, Jennings GT. Nat Rev Immunol 2010;10(11):787–96.
[22] Joshi H, Lewis K, Singharoy A, Ortoleva PJ. Vaccine 2013;31(42):4841–7.
[23] Chen XS, Garcea RL, Goldberg I, Casini G, Harrison SC, Rayment VP. Mol Cell 2000;5:557–67.
[24] Guu TSY, Liu Z, Ye Q, Mata DA, Li K, Yin C, et al. Proc Natl Acad Sci USA 2009;106(31):12992–7.
[25] Wang X, Peng W, Ren J, Hu Z, Xu J, Lou Z, et al. Nat Struct Mol Biol 2012;19(4):424–9.
[26] Miller ST, Hogle JM, Filman DJ. J Mol Biol 2001;307(2):499–512.
[27] Grant RA, Hiremath CN, Filman DJ, Syed R, Andries K, Hogle JM. Curr Biol 1994;4(9):784–97.
[28] Berman HM. Nucleic Acids Res 2000;28(1):235–42.
[29] Carrillo-Tripp M, Shepherd CM, Borelli IA, Venkataraman S, Lander G, Natarajan P, et al. Nucleic Acids Res 2009;37(Database issue):D436–42.
[30] Jorgensen WL. J Am Chem Soc 1981;103(2):335–40.
[31] Humphrey W, Dalke A, Schulten K. J Mol Graph 1996;14(1):33–8.
[32] Martyna GJ, Tobias DJ, Klein ML. J Chem Phys 1994;101:4177.
[33] Phillips JC, Braun R, Wang W, Gumbart J, Tajkhorshid E, Villa E, et al. J Comput Chem 2005;26(16):1781–802.
[34] MacKerell AD, Bashford D, Bellott M, Dunbrack RL, Evanseck JD, Field MJ, et al. J Phys Chem B 1998;102(18):3586–616.
[35] Berendsen HJC, Grigera JR, Straatsma TP. J Phys Chem 1987;91(24):6269–71.
[36] Van Der Spoel D, Lindahl E, Hess B, Groenhof G, Mark AE, Berendsen HJC. J Comput Chem 2005;26(16):1701–18.
[37] Schmid N, Eichenberger AP, Choutko A, Riniker S, Winger M, Mark AE, et al. Eur Biophys J 2011;40(7):843–56.
[38] Bussi G, Donadio D, Parrinello M. J Chem Phys 2007;126(1):014101.
[39] Parrinello M. J Appl Phys 1981;52(12):7182.
[40] Hess B, Bekker H, Berendsen HJC, Fraaije JGEM. J Comput Chem 1997;18(12):1463–72.
[41] Ofek G, Guenaga FJ, Schief WR, Skinner J, Baker D, Wyatt R, et al. Proc Natl Acad Sci USA 2010;107(42):17880–7.
[42] Yokoyama M, Naganawa S, Yoshimura K, Matsushita S, Sato H. PLoS One 2012;7(5):e37530.
[43] Krishnan L, Lomash S, Raj BPJ, Kaur KJ, Salunke DM. J Immunol 2007;178(12):7923–31.
[44] Singharoy A, Polavarapu A, Joshi H, Baik M, Ortoleva P. J Am Chem Soc 2013;135:18458–68.
[45] Kwong PD, Doyle ML, Casper DJ, Cicala C, Leavitt SA, Majeed S, et al. Nature 2002;420(6916):678–82.
[46] Allen TW, Andersen OS, Roux B. J Gen Physiol 2004;124(6):679–90.
[47] Fuglebakk E, Echave J, Reuter N. Bioinformatics 2012;28(19):2431–40.
[48] Connolly ML. J Appl Crystallogr 1983;16(5):548–58.
[49] Zhu F-C, Zhang J, Zhang X-F, Zhou C, Wang Z-Z, Huang S-J, et al. Lancet 2010;376(9744):895–902.
[50] Im SWK, Zhang JZ, Zhuang H, Che XY, Zhu WF, Xu GM, et al. Vaccine 2001;19(27):3726–32.
[51] Li F, Riddell MA, Seow H, Takeda N, Miyamura T, Anderson DA. J Med Virol 2000;386:379–86.
[52] Chou AH, Liu CC, Chang JY, Lien SP, Guo MS, Tasi HP, et al. Clin Dev Immunol 2012;2012.
[53] Liu C-C, Chou A-H, Lien S-P, Lin H-Y, Liu S-J, Chang J-Y, et al. Vaccine 2011;29(26):4362–72.
[54] Dernick R, Heukeshoven J, Hilbrig M. Virology 1983;130(1):243–6.
[55] Chow M, Baltimore D. Proc Natl Acad Sci USA 1982;79(December):7518–21.
[56] Rombaut B, Jore JP. J Gen Virol 1997;78(Pt 8):1829–32.
[57] Rombaut B. Virology 2001;307(1990):305–7.
[58] Chow M, Yabrov R, Bittle J, Hogle J, Baltimore D. Proc Natl Acad Sci USA 1985;82(3):910–4.
[59] Road M, Standards B, Lane B, Mimms S, Bar P, Road L. Plasmid 1989:1453–63.
[60] Ren J, Liu Q, Ellis J, Li J. Bioinformatics 2014;30(12):i264–73.
[61] Yao B, Zheng D, Liang S, Zhang C. PLoS One 2013;8(4):e62249.
[62] Schiffner T, Kong L, Duncan CJA, Back JW, Benschop JJ, Shen X, et al. J Virol 2013;87(18):10163–72.